Available online at www.sciencedirect.com
ScienceDirect
Comput. Methods Appl. Mech. Engrg. 284 (2015) 521–540
Computer methods in applied mechanics and engineering
www.elsevier.com/locate/cma

Variationally consistent domain integration for isogeometric analysis

M. Hillman, J.S. Chen*, Y. Bazilevs

Department of Structural Engineering, University of California, San Diego, 9500 Gilman Drive, La Jolla, CA 92093-0085, United States

Available online 8 November 2014

Abstract

Spline-type approximations for solving partial differential equations are the basis of isogeometric analysis. While the common approach of using integration cells defined by single knot spans using standard (e.g., Gaussian) quadrature rules is sufficient for accuracy, more efficient domain integration is still in high demand. The recently introduced concept of variational consistency provides a guideline for constructing accurate and convergent methods requiring fewer quadrature points than standard integration techniques. In this work, variationally consistent domain integration is proposed for isogeometric analysis. Test function gradients are constructed to meet the consistency conditions, which only requires solving small linear systems of equations. The proposed approach allows for significant reduction in the number of quadrature points employed while maintaining the stability, accuracy, and optimal convergence properties of higher-order quadrature rules. Several numerical examples are provided to illustrate the performance of the proposed domain integration technique.

Keywords: Isogeometric analysis; Domain integration; Quadrature; Integration constraint; Variationally consistent integration

1. Introduction

Isogeometric analysis (IGA) [1,2] provides a way to link Computer Aided Design (CAD) descriptions of designs directly to analysis, circumventing the lengthy and thus expensive process of producing a suitable discretization, as well as bypassing interaction with CAD descriptions for refinement. It also offers several advantages over traditional finite element analysis such as exact descriptions of geometry, more accuracy per degree of freedom in smooth problems [3], and more favorable transient properties [4], among others. However as with any method cast in the Galerkin framework, numerical integration invariably must be considered since high order quadrature can render numerical methods impractical for analysis.

Spline-, and, in particular, Non-Uniform Rational B-Spline (NURBS)-type approximations for solving partial differential equations (PDEs) are the basis of IGA. B-splines, which form the basis of NURBS, are piece-wise polynomial functions. However, the projected geometry yields approximations that are piece-wise rational and are thus more difficult to integrate than polynomials. The parametric description itself can also become an issue when the mapping from the parametric to spatial domain is not affine with large variations in the Jacobian. The widely adopted approach for domain integration in IGA has been to integrate over cells defined by non-zero knot spans or "elements" using Gaussian quadrature [1], with rules sufficient for exact integration of B-splines with affine mapping.

* Corresponding author.
E-mail address: js-chen@ucsd.edu (J.S. Chen).

http://dx.doi.org/10.1016/j.cma.2014.10.004
0045-7825/

However, this procedure is computationally expensive and has been shown to be suboptimal due to the smoothness of the approximation across cell boundaries [5]. While these cell-by-cell integration rules provide accurate domain integration, quadrature rules that provide the same level of accuracy with fewer quadrature points are in demand [5,6].

One approach that has been taken in IGA to alleviate the issue of higher-order quadrature is to use "macro" integration cells, composed of several cells in each parametric direction, with quadrature rules designed to take into account basis-function continuity across constituent cell boundaries [5]. This resulted in a reduction of the number of quadrature points over conventional Gaussian quadrature, and led to the rules that are "optimal" in the sense they can exactly integrate, with the minimum number of points, the integrands they were designed for, namely, 1D B-splines in the parametric domain. Another approach has been to obtain rules using the translation invariant property of B-splines, with only small non-linear systems of equations to solve in order to obtain quadrature point locations and weights [6]. This results in "nearly optimal" quadrature rules, however, these are only applicable to uniform, structured-mesh configurations. A more unified and less restrictive approach is thus desirable, particularly since unstructured-mesh approximations such as T-splines [7], PHT-splines [8], and locally-refined splines [9] are being rapidly developed and adopted for IGA.

Alternative approaches have been taken outside of IGA in order to alleviate quadrature issues. In particular, in the meshfree method, inefficient domain integration can render the method ineffective, and novel domain integration techniques have been developed to overcome this issue. Rather than redesigning quadrature rules for a given approximation space, test and trial functions are constructed so that accuracy and convergence are achieved with lower order quadrature than would otherwise be required. The approach that is becoming increasingly developed is to impose exactness on the Galerkin method with quadrature for the order of approximation space chosen (cf. [10–12]). The basic idea is that assuming completeness of the trial functions, any solution error when solving a boundary value problem with a solution the same as the completeness order is purely due to numerical integration. Setting the residual of the resulting Galerkin equation as zero results in the so-called integration constraint, and satisfaction of the constraint (Galerkin exactness) in addition to the chosen completeness is taken as a criterion to design the test and trial functions. The earliest example of this technique is the stabilized conforming nodal integration (SCNI) method [10], which has proved to be extremely effective at solving a variety of problems [10,13–16], and has also been applied to other methods such as the natural element method [17]. In this method, nodal integration is employed, and gradients are constructed at the nodes using strain smoothing in order to meet the first order integration constraint for first order Galerkin exactness. More recently, extensions of the strain smoothing technique have been proposed in [11] which meet higher-order constraints.

The above methods fall under the framework of the variational consistency condition proposed in [12]. The condition precisely describes what is necessary in order to obtain nth-order exactness in the Galerkin solution, and is thus an extension of the work in [10]. The work in [12] shows that the quadrature treatment of the integration-by-parts performed starting from the weighted residual of a PDE induces error in the discrete solution. This fact, in turn, may be used as a guideline in constructing quadrature rules (or approximation functions) for a given PDE with far fewer quadrature points than standard techniques and without sacrificing stability and optimal convergence. The authors proposed to construct test functions that meet the integration constraint while keeping the trial functions unmodified to ensure completeness. In this work, variationally consistent domain integration is proposed for IGA. Quadrature cells are defined by non-zero knot spans, and test functions are constructed to meet the variational consistency condition. The method is shown to produce the accuracy of the Galerkin technique with higher-order quadrature while using far fewer integration points. In some cases *one quadrature point per basis function* (for a scalar problem) is employed without degradation of convergence, making the method comparable in computational cost to a collocation technique [18–20].

The remainder of this paper is as follows. Section 2 gives a brief overview of NURBS-based IGA, with a discussion of the properties of the approximation functions relevant to domain integration. The concept of variational consistency is then introduced in Section 3, with emphasis placed on its application to IGA. Numerical examples are then given in Section 4. Concluding remarks are then given in Section 5.

2. NURBS-based IGA

In this section, the NURBS-based isogeometric method is briefly reviewed. Properties of the basis functions relevant to domain integration are also discussed.

2.1. B-splines and NURBS

B-splines and NURBS form the basis of IGA, motivated by CAD descriptions of geometry. A B-spline is a piece-wise polynomial curve, constructed by a linear combination of n basis functions of order p and the associated n coefficients called control points.

2.1.1. Knots and knot vectors

B-splines are built upon a knot vector, which consists of a set of points ξ_i with non-decreasing coordinates in the parametric space, called *knots*. The points are not necessarily unique, and when they have the same coordinates they are said to be *repeated knots*. In the standard CAD descriptions, and what has been adopted in IGA and will be employed here, knots are repeated $p+1$ times at the ends of the parametric space, and such knot vectors are called *open knot vectors*.

2.1.2. B-spline basis functions

The basis functions of B-splines can be defined by a recursive construction, starting with piece-wise constant functions for $p = 0$:

$$N_{i,0}(\xi) = \begin{cases} 1 & \text{if } \xi_i \leq \xi < \xi_{i+1} \\ 0 & \text{otherwise} \end{cases} \tag{1}$$

and for $p > 0$

$$N_{i,p}(\xi) = \frac{\xi - \xi_i}{\xi_{i+p} - \xi_i} N_{i,p-1}(\xi) + \frac{\xi_{i+p+1} - \xi}{\xi_{i+p+1} - \xi_{i+1}} N_{i+1,p-1}(\xi). \tag{2}$$

For $p = 1$, the basis functions reduce to the linear finite element shape functions. Thus the cases of interest in isogeometric analysis are $p > 1$ since linear finite elements are well established. In addition, quadratic ($p = 2$) bases are the minimum order for resulting NURBS curves to exactly represent many geometries of interest.

2.1.3. B-spline curves, surfaces and solids

A B-spline curve $\boldsymbol{C}(\xi) \in \mathbb{R}^2$ is constructed by the linear combination of basis functions $N_{i,p}(\xi)$ and control point coordinates $\boldsymbol{B}_i$:

$$\boldsymbol{C}(\xi) = \sum_{i=1}^{n} N_{i,p}(\xi) \boldsymbol{B}_i \tag{3}$$

where the basis functions are built upon the knot vector $\boldsymbol{\Xi} = [\xi_1, \quad \ldots, \quad \xi_{p+n+1}]$.

Surfaces and solids are constructed by using tensor products of the basis functions. A surface $\boldsymbol{S}(\xi, \eta) \in \mathbb{R}^3$ thus has bases $N_{i,p}(\xi)$ and $M_{j,q}(\eta)$ with the possibility of having differing order p and q respectively. Associated with these bases is a set of control points $\boldsymbol{B}_{ij}$ called a *control net* with $m \times n$ components, and knot vectors $\boldsymbol{\Xi} = [\xi_1, \quad \ldots, \quad \xi_{p+n+1}]$ and $\mathbf{H} = [\eta_1, \quad \ldots, \quad \eta_{q+m+1}]$. B-spline surfaces are constructed over the parametric domain $[\xi_1, \xi_{p+n+1}] \times [\eta_1, \eta_{q+m+1}]$:

$$\boldsymbol{S}(\xi, \eta) = \sum_{i=1}^{n} \sum_{j=1}^{m} N_{i,p}(\xi) M_{j,q}(\eta) \boldsymbol{B}_{ij}. \tag{4}$$

B-spline solids are constructed in a manner analogous to (4).

2.2. NURBS

In order to facilitate exact geometric descriptions for objects such as circles, ellipses, and other conic sections, projective transformations of B-splines can be introduced. NURBS are projections of B-splines in $\mathbb{R}^{d+1}$ onto $\mathbb{R}^d$, resulting in a piece-wise rational function.

For a curve, the control points $\boldsymbol{B}_i^w$ defining the curve in $\mathbb{R}^{d+1}$ are projected to give the NURBS control points

$$(\boldsymbol{B}_i)_j = \frac{\left(\boldsymbol{B}_i^w\right)_j}{w_i}, \quad j = 1, \ldots, d \tag{5}$$

where j denotes the component, and $w_i = (\boldsymbol{B}_i^w)_{d+1}$ is the last component of the projective control points, and is called the weight of $\boldsymbol{B}_i$. The bases associated with each control point are also projected yielding

$$R_i^p(\xi) = \frac{N_{i,p}(\xi) w_i}{\sum_{\bar{i}=1}^{n} N_{\bar{i},p}(\xi) w_{\bar{i}}}. \tag{6}$$

The NURBS curve is then defined as

$$\boldsymbol{C}(\xi) = \sum_{i=1}^{n} R_i^p(\xi) \boldsymbol{B}_i. \tag{7}$$

Here it can be seen that when the weights in (6) are non-uniform, the basis functions are rational, and in coarse descriptions of geometry weights can vary significantly over the knot spans. When refined, weights become more uniform since the projective control points move closer to each other. As the weights become uniform, the functions locally approach the form of B-splines.

For surfaces, NURBS basis functions are defined as

$$R_{i,j}^{p,q}(\xi, \eta) = \frac{N_{i,p}(\xi) M_{j,q}(\eta)}{\sum_{\bar{i}=1}^{n} \sum_{\bar{j}=1}^{m} N_{\bar{i},p}(\xi) M_{\bar{j},q}(\eta) w_{\bar{i}\bar{j}}}. \tag{8}$$

The construction of surfaces and solids are performed analogous to (7). In what follows, the superscripts such as those in (6) and (8) will be dropped with an equal order p, and the subscripts will be defined with respect to a single index in relation to the total number of control points.

2.3. IGA and domain integration

IGA provides a link between CAD-based geometric descriptions and the approximated solutions of PDEs, where the bases used to represent the geometry are also used directly as the bases in the Galerkin approximation. The so-called affine covariance property ensures that the constant and linear completeness of NURBS are inherited from the B-splines themselves, and thus allows exact representations of rigid body modes, as well as constant stress and strain states in elasticity [1].

The integrands appearing in the weak form however, present difficulty for formulating efficient quadrature rules owing to the nature of the approximation functions employed. Higher order integration is often required for sufficient accuracy when using standard integration techniques for rational shape functions such as those in (6), which is particularly problematic in coarser descriptions of geometry since weights are less uniform with respect to knot spans than in the refined models. The mapping involved in the isogeometric approach may also become an issue when it deviates from affine. Again this may be problematic for coarse discretizations as large variations in non-affine mapping can exist over integration cells. Cell-by-cell integration with sufficiently high order Gaussian quadrature can overcome these issues, but on the other hand, consumes high CPU.

3. Variationally consistent integration

In this section the concept of variational consistency is reviewed, and its implications for IGA are discussed. Specifics of using the variational consistency conditions as a correction for IGA for enhanced accuracy and convergence are also given.

3.1. Variational consistency for scalar equations

High order integration ensures accuracy and convergence in the Galerkin method, but may not be viable due to the associated cost. To avoid the bottleneck, which may occur in certain classes of methods, an alternative to higher-order integration has been offered in [12], cast under the framework of satisfaction of variational consistency conditions. The consistency conditions dictate precisely what is necessary in order to achieve arbitrary-order Galerkin exactness. These conditions serve to characterize the solution error due to quadrature inaccuracy when approximation functions are sufficient for representing the true solution, since any solution error in this case is purely due to numerical integration.

Consider the Poisson equation as a model problem:

$$\begin{aligned} &\nabla^2 u + s = 0 \quad \text{in } \Omega \\ &\mathbf{n}\cdot\nabla u = h \quad \text{on } \partial\Omega_h \\ &u = g \quad \text{on } \partial\Omega_g. \end{aligned} \tag{9}$$

The Galerkin form of (9) can be stated to find $(u^h, \lambda^h) \in U^h \times \Lambda^h$, such that for all $(v^h, \gamma^h) \in V^h \times \Gamma^h$ the following equation holds:

$$\int_\Omega \nabla v^h \cdot \nabla u^h \,\mathrm{d}\Omega = \int_\Omega v^h s \,\mathrm{d}\Omega + \int_{\partial\Omega_h} v^h h \,\mathrm{d}\Gamma + \int_{\partial\Omega_g} v^h \lambda^h \,\mathrm{d}\Gamma + \int_{\partial\Omega_g} \gamma^h (u^h - g) \,\mathrm{d}\Gamma \tag{10}$$

where $U^h \subset H^1$, $V^h \subset H^1$, $\Lambda^h \subset L^2$, and $\Gamma^h \subset L^2$ are suitable finite-dimensional subspaces. Here, for illustration, Lagrange multipliers have been employed for enforcement of essential boundary conditions, however what follows applies to all enforcements which are consistent with the strong form of the problem.

Consider the employment of NURBS as approximations and suitable Lagrange multipliers:

$$\begin{aligned} u^h &= \sum_{I=1}^{NP} R_I u_I, \qquad v^h = \sum_{I=1}^{NP} \hat{R}_I v_I \\ \lambda^h &= \sum_{I=1}^{NC} \varphi_I \lambda_I, \qquad \gamma^h = \sum_{I=1}^{NC} \hat{\varphi}_I \gamma_I \end{aligned} \tag{11}$$

where NP is the dimension of the primary variable (the number of control points), and NC is the dimension of the functions associated with enforcement of the essential boundary conditions. Employing numerical integration and substituting the approximations in (11), the discrete version of (10) is thus

$$\begin{aligned} \sum_{J=1}^{NP} \hat{\int_\Omega} \nabla \hat{R}_I \cdot \nabla R_J u_J \,\mathrm{d}\Omega = &\hat{\int_\Omega} \hat{R}_I s \,\mathrm{d}\Omega + \hat{\int_{\partial\Omega_h}} \hat{R}_I h \,\mathrm{d}\Gamma + \sum_{J=1}^{NC} \hat{\int_{\partial\Omega_g}} \hat{R}_I \varphi_J \lambda_J \,\mathrm{d}\Gamma \\ &+ \hat{\int_{\partial\Omega_g}} \hat{\varphi}_K \left(\sum_{J=1}^{NP} R_J u_J - g \right) \mathrm{d}\Gamma \quad \forall\, I, \forall K. \end{aligned} \tag{12}$$

In the above, the integral symbols with "$\hat{}$" denote numerical integration. Consider now the case when the solution of (9) is complete monomials with degree n:

$$u = \sum_{|\alpha|\le n} \boldsymbol{c}_\alpha \mathbf{x}^\alpha \equiv u^n. \tag{13}$$

Here we have introduced the multi-index notation $\alpha = (\alpha_1, \alpha_2, \ldots, \alpha_d)$, with the length of α defined as $|\alpha| = \sum_{i=1}^d \alpha_i$, and $\mathbf{x}^\alpha \equiv x_1^{\alpha_1} \cdot x_2^{\alpha_2} \cdot \ldots \cdot x_d^{\alpha_d}$. To design (9) with the solution u^n, the conditions are prescribed as

$$\begin{aligned} &s = -\nabla^2 u^n \quad \text{in } \Omega \\ &h = \nabla u^n \cdot \mathbf{n} \quad \text{on } \partial\Omega_h \\ &g = u^n \text{on } \partial\Omega_g. \end{aligned} \tag{14}$$

Note using the equivalence of strong and weak forms, the Lagrange multiplier for this solution is $\lambda^n = \nabla u^n \cdot \mathbf{n}$. Considering (12) with the solution u^n, Lagrange multiplier λ^n, and using the associated prescribed boundary conditions in (14), the resulting equation is

$$\int_{\Omega} \nabla \hat{R}_I \cdot \nabla u^n \, \mathrm{d}\Omega = \int_{\Omega} \hat{R}_I s \, \mathrm{d}\Omega + \int_{\partial \Omega_h} \hat{R}_I h \, \mathrm{d}\Gamma + \int_{\partial \Omega_g} \hat{R}_I \lambda^n \, \mathrm{d}\Gamma \quad \forall I. \tag{15}$$

Using the definition of the Lagrange multiplier $\lambda^n = \nabla u^n \cdot \mathbf{n}$ associated with u^n, and the remaining conditions in (14) we then have

$$\int_{\Omega} \nabla \hat{R}_I \cdot \nabla u^n \, \mathrm{d}\Omega = - \int_{\Omega} \hat{R}_I \nabla^2 u^n \, \mathrm{d}\Omega + \int_{\partial \Omega} \hat{R}_I \nabla u^n \cdot \mathbf{n} \, \mathrm{d}\Gamma \quad \forall I. \tag{16}$$

Finally, considering the arbitrary constants in (13) gives

$$\int_{\Omega} \nabla \hat{R}_I \cdot \nabla \mathbf{x}^{\alpha} \, \mathrm{d}\Omega = - \int_{\Omega} \hat{R}_I \nabla^2 \mathbf{x}^{\alpha} \, \mathrm{d}\Omega + \int_{\partial \Omega} \hat{R}_I (\nabla \boldsymbol{x}^{\alpha} \cdot \mathbf{n}) \, \mathrm{d}\Gamma \quad \forall I, \ \ |\alpha| = 0, 1, \ldots, n. \tag{17}$$

Domain integration that meets (17) yields Galerkin exactness of order n and has been termed variationally consistent integration (VCI) [12]. Methods which possess nth-order completeness and satisfy (17) are able to pass the nth order patch tests for (9). The conditions state that the numerical integration should be consistent with the test functions in the form of the integration by parts operations associated with the PDE at hand. Thus the condition illustrates that the integration by parts involved in the weak form introduces error into the solution when inexact quadrature is used.

The completeness requirement is an obvious strict necessity for exactness: the solution we wish to obtain must lie in the approximation space at hand. For IGA, nth order completeness for B-splines is only satisfied in the parametric domain [21]. In the spatial domain only first-order completeness is guaranteed for IGA, which is due to the isoparametric construction employed. Nevertheless, despite the lack of nth order completeness in the spatial domain, optimal convergence for NURBS-based IGA was rigorously shown in [22]. As a result, the IGA approximation functions employed are considered sufficient for solution representation, and test functions can be constructed based on (17) to reduce the integration error while keeping the trial functions unmodified. The use of condition given by (17) to construct test functions for IGA assumes that the error due to the lack of global higher-order completeness is small compared to the error due to quadrature. The results in Section 4 show that variational consistency is indeed an effective technique for correcting integration error, and that the lack of global higher-order completeness generally does not affect the performance of the method.

It is important to note that unlike in more standard approaches of quadrature rule design, which seek to find the quadrature point locations and weights to maximize accuracy, here it is assumed that a quadrature rule is given and an appropriate modification to the test function space can be introduced to ensure that the resulting numerical scheme has good convergence properties.

To make (17) more concrete, consider $n = 1$, which results in

$$\int_{\Omega} \nabla \hat{R}_I \, \mathrm{d}\Omega = \int_{\partial \Omega} \hat{R}_I \mathbf{n} \, \mathrm{d}\Gamma \quad \forall I. \tag{18}$$

Thus the linear case simplifies to a divergence condition for the test function $\hat{R}_I$, which was the condition originally derived in [10]. The conditions in (17) for $n = 2$ for the 2D case are

$$\begin{aligned}
\int_{\Omega} \hat{R}_{I,1} x \, \mathrm{d}\Omega &= - \int_{\Omega} \hat{R}_I \, \mathrm{d}\Omega + \int_{\partial \Omega} \hat{R}_I x n_1 \, \mathrm{d}\Gamma \quad \forall I \\
\int_{\Omega} \hat{R}_{I,2} y \, \mathrm{d}\Omega &= - \int_{\Omega} \hat{R}_I \, \mathrm{d}\Omega + \int_{\partial \Omega} \hat{R}_I y n_2 \, \mathrm{d}\Gamma \quad \forall I \\
\int_{\Omega} \left(\hat{R}_{I,1} y + \hat{R}_{I,2} x \right) \mathrm{d}\Omega &= \int_{\partial \Omega} \hat{R}_I \left(y n_1 + x n_2 \right) \mathrm{d}\Gamma \quad \forall I.
\end{aligned} \tag{19}$$

Note that for nth-order exactness, each constraint from order 0 to n should be satisfied.

3.2. Variational consistency for vector equations

Consider the following nth-order displacement field $\mathbf{u} = \sum_{|\alpha|\leq n} \mathbf{c}_\alpha \mathbf{x}^\alpha \equiv \mathbf{u}^n$ for the elasticity problem

$$\begin{aligned} &\boldsymbol{\nabla}\cdot\boldsymbol{\sigma} + \mathbf{b} = \mathbf{0} \quad \text{in } \Omega \\ &\boldsymbol{\sigma}\cdot\mathbf{n} = \mathbf{h} \quad \text{on } \partial\Omega_h \\ &\mathbf{u} = \mathbf{g} \quad \text{on } \partial\Omega_g. \end{aligned} \tag{20}$$

The Cauchy stress tensor corresponding to the displacement field $\mathbf{u}^n$ is $\boldsymbol{\sigma} = \mathbf{C} : \boldsymbol{\nabla}^s\mathbf{u}^n \equiv \boldsymbol{\sigma}^n$ where $\mathbf{C}$ is the elasticity tensor, and $\boldsymbol{\nabla}^s\mathbf{u} = 1/2\,(\boldsymbol{\nabla}\otimes\mathbf{u} + \mathbf{u}\otimes\boldsymbol{\nabla})$ is the strain tensor. The conditions in (20) for the nth-order patch test are $\mathbf{b} = -\boldsymbol{\nabla}\cdot\boldsymbol{\sigma}^n$ in Ω, $\mathbf{h} = \boldsymbol{\sigma}^n\cdot\mathbf{n}$ on $\partial\Omega_h$, and $\mathbf{g} = \mathbf{u}^n$ on $\partial\Omega_g$.

The integration constraints for elasticity can be obtained following similar procedures for the scalar equations:

$$\hat{\int_\Omega} \boldsymbol{\nabla}\hat{R}_I\cdot\boldsymbol{\sigma}^\alpha \,\mathrm{d}\Omega = -\hat{\int_\Omega} \hat{R}_I\boldsymbol{\nabla}\cdot\boldsymbol{\sigma}^\alpha \,\mathrm{d}\Omega + \hat{\int_{\partial\Omega}} \hat{R}_I\boldsymbol{\sigma}^\alpha\cdot\mathbf{n}\,\mathrm{d}\Gamma \quad \forall I,\ |\alpha| = 0, 1, \ldots, n \tag{21}$$

where $\boldsymbol{\sigma}^\alpha = \mathbf{C} : \boldsymbol{\nabla}^s\mathbf{x}^\alpha$.

Reduction of (21) for $n = 1$ gives the divergence condition (18). For quadratic exactness ($n = 2$), in 2D, there are four conditions rather than three found in the Poisson equation:

$$\begin{aligned} \hat{\int_\Omega} \hat{R}_{I,1}x \,\mathrm{d}\Omega &= -\hat{\int_\Omega} \hat{R}_I \,\mathrm{d}\Omega + \hat{\int_{\partial\Omega}} \hat{R}_I x n_1 \,\mathrm{d}\Gamma \quad \forall I \\ \hat{\int_\Omega} \hat{R}_{I,2}y \,\mathrm{d}\Omega &= -\hat{\int_\Omega} \hat{R}_I \,\mathrm{d}\Omega + \hat{\int_{\partial\Omega}} \hat{R}_I y n_2 \,\mathrm{d}\Gamma \quad \forall I \\ \hat{\int_\Omega} \hat{R}_{I,2}x \,\mathrm{d}\Omega &= \hat{\int_{\partial\Omega}} \hat{R}_I x n_2 \,\mathrm{d}\Gamma \quad \forall I \\ \hat{\int_\Omega} \hat{R}_{I,1}y \,\mathrm{d}\Omega &= \hat{\int_{\partial\Omega}} \hat{R}_I y n_1 \,\mathrm{d}\Gamma \quad \forall I. \end{aligned} \tag{22}$$

3.3. Variationally consistent integration

In general, variational consistency is not satisfied given an approximation space and a type of quadrature. In variationally consistent integration, the trial functions play the role of completeness, while the test functions and quadrature rules are responsible for meeting the integration constraint (17). Given a set of approximation functions, the integration constraints in (17) can be separately imposed on the test functions $\hat{R}_I$. The procedure given in [12] is to introduce a correction to the test function gradients. Specifically, a direct gradient and an assumed gradient are introduced for the trial and test functions, respectively. For isoparametric methods the question arises whether to construct corrections in the parametric domain or in the spatial domain. Here, since the conditions are enforced in the spatial domain, the correction is defined in the spatial domain. The use of both ensures the attractive properties of the corrections introduced in [12] are maintained; the VCI equations are uncoupled (reducing the size of the equations by a factor of the spatial dimension d), whereas for parametric corrections this is not straightforward to achieve. In addition, the resulting matrix of coefficients is symmetric and positive definite so long as the correction functions have sufficient support cover over the integration points.

The starting point for the parametrically defined NURBS is to compute parametric derivatives $\boldsymbol{\nabla}_{\boldsymbol{\xi}}$ directly, and spatial derivatives $\boldsymbol{\nabla}$ (denoted with no subscripts) necessary for the weak form are then obtained using the Jacobian matrix. A corrected gradient is then introduced to these test function derivatives:

$$\tilde{\boldsymbol{\nabla}} v^h = \sum_{I=1}^{NP} \left(\boldsymbol{\nabla} R_I + \sum_{|\beta|\leq n} \chi_{\beta I} \boldsymbol{\Psi}_I^\beta \right) v_I. \tag{23}$$

In the above, $\{\boldsymbol{\Psi}_I^\beta\}_{|\beta|=1}^n$ is a set of additional basis functions with $\{\nabla R_I, \boldsymbol{\Psi}_I^\beta\}_{|\beta|=1}^n$ linearly independent, and $\chi_{\beta I}$ are coefficients which are solved for by substitution of (23) into the integration constraints (17). The number of unknown coefficients in (23) is equal to the number of integration constraints in (17), and the gradient correction can be formed by solving the resulting linear system. The corrected gradient approach simplifies the correction equations over a direct gradient approach, reduces computational cost, and also provides stability under sufficient conditions (see [12]).

Note that all polynomial terms in (17) are simply evaluated by the map $\mathbf{x}(\boldsymbol{\xi})$, i.e.,

$$\int_\Omega f(\mathbf{x})\,\mathrm{d}\Omega = \int_\square f(\mathbf{x}(\boldsymbol{\xi}))J(\boldsymbol{\xi})\,\mathrm{d}\Omega \tag{24}$$

where $J(\boldsymbol{\xi})$ is the Jacobian of the mapping.

It is possible to uncouple the equations resulting from (23) for computational efficiency. To take a simple example, consider a correction in 2D for satisfaction of the linear constraint equation (18):

$$\tilde{\nabla} v^h = \sum_{I=1}^{NP}\left(\nabla R_I + \chi_{1I}\begin{Bmatrix}\Phi_I\\0\end{Bmatrix} + \chi_{2I}\begin{Bmatrix}0\\\Phi_I\end{Bmatrix}\right) v_I. \tag{25}$$

Here Φ_I is taken in a simple form as

$$\Phi_I(\boldsymbol{\xi}) = \begin{cases}1 & \text{if } \boldsymbol{\xi}\in \mathrm{supp}(R_I)\\ 0 & \text{if } \boldsymbol{\xi}\notin \mathrm{supp}(R_I).\end{cases} \tag{26}$$

With substitution into (18), the coefficients are solved for directly from the resulting scalar equations:

$$\begin{aligned}\chi_{1I} &= \left(\int_{\partial\hat{\Omega}} \hat{R}_I n_1\,\mathrm{d}\Gamma - \int_{\hat{\Omega}} \hat{R}_{I,1}\,\mathrm{d}\Omega\right)\Big/\left(\int_{\hat{\Omega}}\Phi_I\,\mathrm{d}\Omega\right)\\ \chi_{2I} &= \left(\int_{\partial\hat{\Omega}} \hat{R}_I n_2\,\mathrm{d}\Gamma - \int_{\hat{\Omega}} \hat{R}_{I,2}\,\mathrm{d}\Omega\right)\Big/\left(\int_{\hat{\Omega}}\Phi_I\,\mathrm{d}\Omega\right).\end{aligned} \tag{27}$$

It can be seen that the above correction is driven by the residual of (18), and thus no correction is made to methods which are already first-order variationally consistent, for example, stabilized conforming nodal integration [10].

For higher order corrections, it is convenient to adopt a matrix representation of the constraints (17). For the elasticity and Poisson problems in d-dimensions, it is sufficient to consider a vector $\mathbf{P}$ containing the complete $(n-1)$th order monomials for the constraints:

$$\int_{\hat{\Omega}} \mathbf{P}^T \hat{R}_{I,i}\,\mathrm{d}\Omega = -\int_{\hat{\Omega}} \mathbf{P}_{,i}^T \hat{R}_I\,\mathrm{d}\Omega + \int_{\partial\hat{\Omega}} \mathbf{P}^T \hat{R}_I n_i\,\mathrm{d}\Gamma \quad \forall I,\ i=1,\ldots,d. \tag{28}$$

Test function gradients are then introduced with a monomial of the same order, with coefficients determined by satisfaction of (28):

$$\hat{R}_{I,i} = R_{I,i} + \mathbf{P}\boldsymbol{\chi}_{iI}\Phi_I, \quad i=1,\ldots,d \tag{29}$$

where $\boldsymbol{\chi}_{iI} = [\chi_{iI1}, \quad \ldots, \quad \chi_{iI|\alpha|}]^T$. Inserting the test functions into the integration constraint (28) yields

$$\mathbf{A}_I\boldsymbol{\chi}_{iI} = \mathbf{r}_{iI} \tag{30}$$

where

$$\begin{aligned}\mathbf{r}_{iI} &= -\int_{\hat{\Omega}} \mathbf{P}^T R_{I,i}\,\mathrm{d}\Omega - \int_{\hat{\Omega}} \mathbf{P}_{,i}^T R_I\,\mathrm{d}\Omega + \int_{\partial\hat{\Omega}} \mathbf{P}^T R_I n_i\,\mathrm{d}\Gamma\\ \mathbf{A}_I &= \int_{\hat{\Omega}} \mathbf{P}^T\mathbf{P}\Phi_I\,\mathrm{d}\Omega.\end{aligned} \tag{31}$$

It can be seen that $\mathbf{r}_{iI}$ is the residual of the integration constraints (28) and the coefficients solved from (30) correct the integration-constraint violation. Here again it can be seen that the correction is driven directly by the residual, and for variationally consistent methods no correction is applied. The resulting method is variationally consistent to

an arbitrarily high order. Note that since no specific properties of the approximations functions or discretization are invoked, the method is applicable to arbitrary discretizations within IGA and beyond.

It is worth noting what is involved in forming the correction. First, domain or boundary integration is performed for several terms, however, examination of the residual in (31) shows that most terms are already computed in a typical problem. The coefficient matrix on the left-hand-side of (30) is composed of monomials, and is symmetric requiring only the upper or lower triangle to be calculated. All calculations are local because of the compactness of (29) and compactness of the basis functions themselves. After forming the required terms, only a relatively small linear system must be solved for each basis function. The dimension of the system is the number of terms in the complete $(n-1)$th order monomial.

3.4. Variationally consistent reduced integration method

The widely adopted approach for domain integration in IGA has been to integrate over cells defined by non-zero knot spans or "elements" using Gaussian integration, and will be the approach adopted here. The procedure is to generate points for each cell, for which Gauss points are defined on their standard domain. These points are then mapped to the "global" parametric domain where shape functions are defined, for which each point has a map $\mathbf{F}$ to the spatial domain. The relationship between these systems is illustrated in Fig. 1 for $p = 2$. The usual rule is such that B-splines of degree p with affine mapping can be exactly integrated, giving $p + 1$ integration points per cell in each direction. However, for the problems tested, p integration points per cell have been employed with optimal convergence attained, which is taken for comparison in the next section.

Using VCI, we further reduce the number of quadrature points used on each cell as discussed in what follows. The rules we propose are to use $p - 1$ for $p > 1$ (or, possibly, $p - 2$ for $p > 2$) integration points per element, with p points per element where repeated knots exist (typically near the boundary) to avoid rank deficiency. The integration scheme is then corrected using (29), where we set $n = p$. Various integration schemes with reduced quadrature for $p = 2, 3, 4$ are depicted in Fig. 2 for illustration. Note that for the case $p = 2$ the number of quadrature points equals the number of control points, and, as a result, basis functions. As such, the method is cost-comparable to a collocation technique. Also note that for single-element meshes, $p + 1$ points must be used to obtain full-rank matrices no matter the case, and thus two or more elements in each direction are considered in the examples.

4. Numerical examples

In this section, we present several numerical examples to show the effectiveness of the proposed method. The patch test is first considered, then examples testing the convergence of the method. Nitsche's method is employed for the weak enforcement of essential boundary conditions [23] with a penalty parameter $1.0 \times 10^7/h$, where h is the characteristic length of the discretization, taken as the maximum diagonal of the elements. Herein, the tensor product of rth order Gauss integration (GI) rules for each cell is denoted "$r \times r$ GI", and the proposed reduced rules with $r \times r$ points in elements adjacent to repeated knots and $s \times s$ rules on the rest of the domain are denoted for uncorrected and corrected methods by "$s \times s/r \times r$ GI" and "$s \times s/r \times r$ VC-GI", respectively.

4.1. Poisson equation: patch tests

Consider the Poisson equation designed with the linear solution $u = x + 2y$:

$$\begin{aligned} &\nabla^2 u = 0 \quad \text{in } \Omega \\ &\nabla u \cdot \mathbf{n} = n_1 + 2n_2 \quad \text{on } \partial\Omega_h \\ &u = x + 2y \quad \text{on } \partial\Omega_g \end{aligned} \tag{32}$$

where $\Omega : (0,1) \times (0,1)$, $\partial\Omega_h : 0 \le x \le 1,\ y = 1;\ x = 1,\ 0 \le y \le 1$, $\partial\Omega_g = \partial\Omega \backslash \partial\Omega_h$. Linear NURBS are employed in the computations with 2×2 GI, the proposed VC technique $1 \times 1/2 \times 2$ VC-GI, and its uncorrected counterpart $1 \times 1/2 \times 2$ GI. A uniform discretization is considered with a perturbation factor β that perturbs a coarse four element geometry with

$$\begin{aligned} B_{Ii} &= B^0_{Ii} + 0.4\alpha_{Ii}\beta \\ w_I &= w^0_I + 2\gamma_I\beta \end{aligned} \tag{33}$$

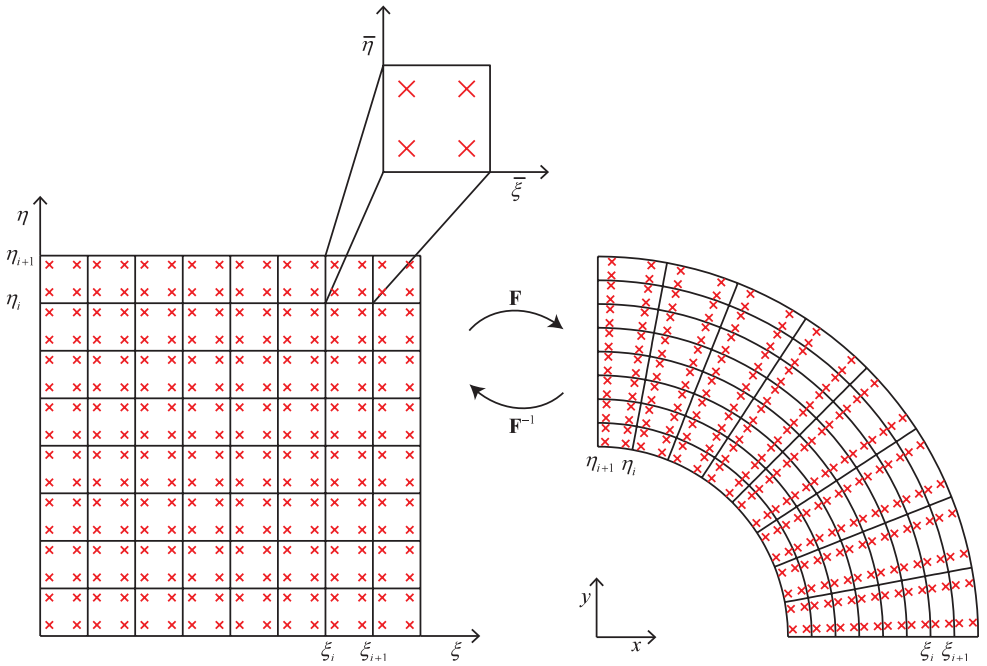

Fig. 1. Generation of Gauss points and relation between domains for $p = 2$.

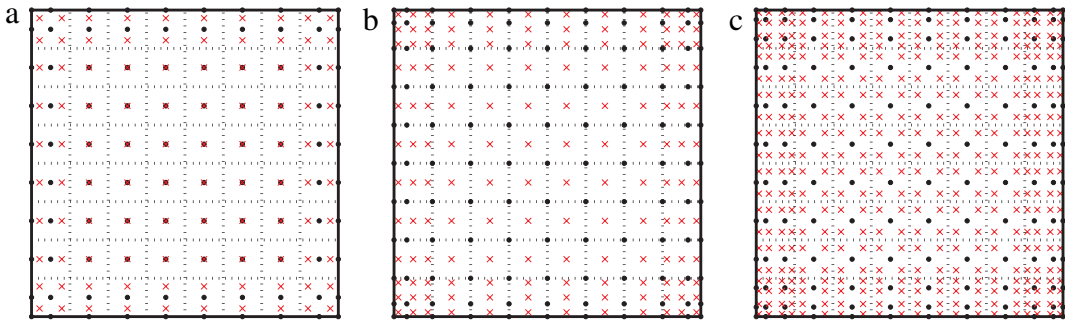

Fig. 2. Integration schemes with maximum reduced quadrature for (a) $p = 2$, (b) $p = 3$, and (c) $p = 4$. Black circles denote control points, red crosses integration points, and dashed lines integration cells.

where B^0_{Ii} and B_{Ii} are the original uniform control points and perturbed control points, respectively, w^0_I and w_I are the original and perturbed weights respectively, and $\alpha_{Ii} \in [-1, 1]$ and $\gamma_I \in [0, 1]$ are random numbers for each I and i and each coarse discretization. The coarse discretization is refined uniformly to produce 16 elements. The discretizations used are shown in Fig. 3 with the integration scheme $1 \times 1/2 \times 2$ VC-GI.

The results for the L^2 norm and H^1 seminorm of the error are shown in Tables 1 and 2, respectively, demonstrating how the variationally consistent method can pass the linear patch test for arbitrary discretizations. Only in the perfectly uniform case can the other methods pass the patch test. The error for 2×2 GI integration is smaller than $1 \times 1/2 \times 2$ GI, which can be fairly significant for all discretizations. However with the employment of VCI, the error can be completely eliminated.

Now consider the Poisson equation designed with a quadratic solution $u = x + 2y + x^2 + 2xy + y^2$:

$$\begin{aligned} &\nabla^2 u = 4 \quad \text{in } \Omega \\ &\nabla u \cdot \mathbf{n} = n_1(1 + 2x + 2y) + 2n_2(1 + x + y) \quad \text{on } \partial\Omega_h \\ &u = x + 2y + x^2 + 2xy + y^2 \quad \text{on } \partial\Omega_g. \end{aligned} \tag{34}$$

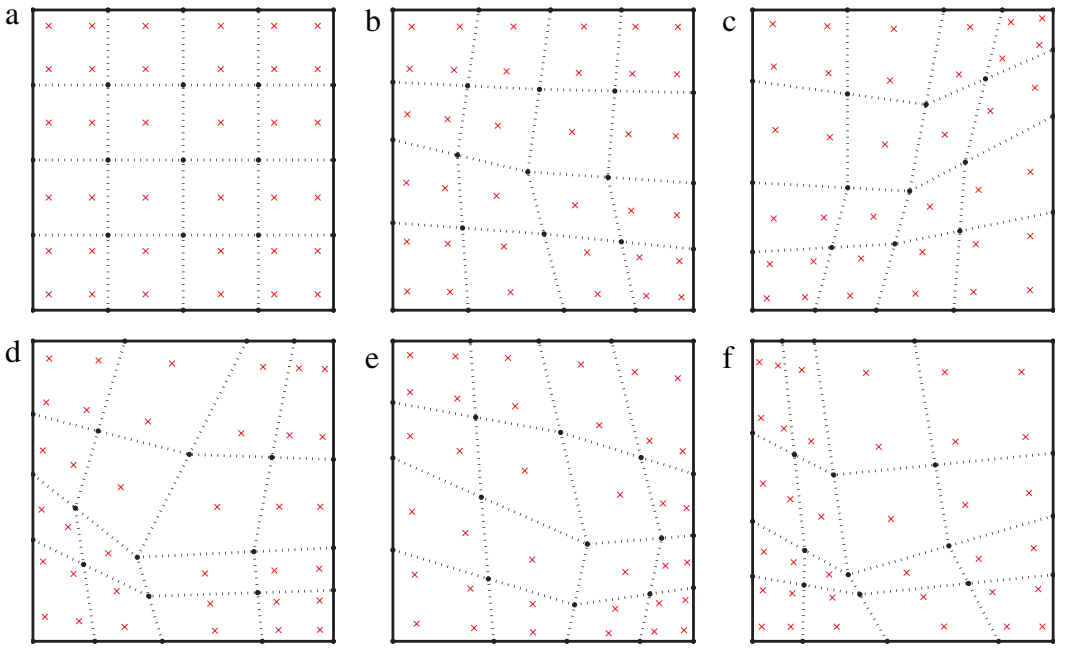

Fig. 3. Integration schemes with reduced quadrature for linear patch test with (a) $\beta = 0.0$, (b) $\beta = 0.2$, (c) $\beta = 0.4$, (d) $\beta = 0.6$, (e) $\beta = 0.8$, and (f) $\beta = 1.0$. Black circles denote control points, red crosses integration points, and dashed lines integration cells.

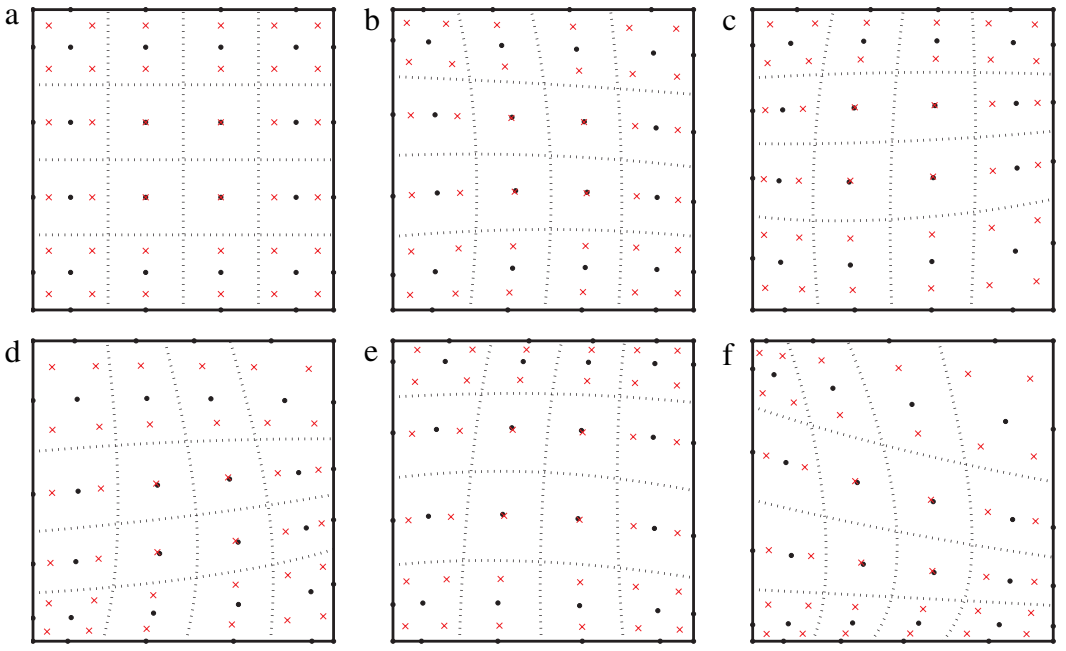

Fig. 4. Integration schemes with reduced quadrature for quadratic patch test with (a) $\beta = 0.0$, (b) $\beta = 0.2$, (c) $\beta = 0.4$, (d) $\beta = 0.6$, (e) $\beta = 0.8$, and (f) $\beta = 1.0$. Black circles denote control points, red crosses integration points, and dashed lines integration cells.

Quadratic NURBS are employed with a uniform single element discretization perturbed by (33) and refined to 16 elements, giving the discretizations shown in Fig. 4, shown with $1 \times 1/2 \times 2$ VC-GI. The integration methods 2×2 GI, $1 \times 1/2 \times 2$ VC-GI, and $1 \times 1/2 \times 2$ GI are employed, using the same boundary conditions as the previous example. The errors in the L^2 norm and H^1 seminorm are shown in Tables 3 and 4, respectively. Here it can be

Table 1
L^2 norm of error in the linear patch test for various methods and discretizations.

Method	β					
	0.0	0.2	0.4	0.6	0.8	1.0
1 × 1/2 × 2 GI	2.65E−16	0.002356	0.003700	0.006858	0.013119	0.010626
1 × 1/2 × 2 VC-GI	2.93E−16	5.76E−16	6.13E−16	3.11E−16	7.69E−16	8.44E−16
2 × 2 GI	8.79E−16	0.000012	0.000079	0.000053	0.000330	0.000283

Table 2
H^1 seminorm of error in the linear patch test for various methods and discretizations.

Method	β					
	0.0	0.2	0.4	0.6	0.8	1.0
1 × 1/2 × 2 GI	2.28E−15	0.021555	0.022446	0.058587	0.086904	0.099351
1 × 1/2 × 2 VC-GI	2.44E−15	2.72E−15	2.49E−15	2.71E−15	3.23E−15	2.52E−15
2 × 2 GI	3.45E−15	0.000043	0.000487	0.000285	0.002351	0.002371

Table 3
L^2 norm of error in the quadratic patch test for various methods and discretizations.

Method	β					
	0.0	0.2	0.4	0.6	0.8	1.0
1 × 1/2 × 2 GI	0.012138	0.011987	0.012270	0.017855	0.017810	0.022055
1 × 1/2 × 2 VC-GI	9.45E−16	0.000529	0.000736	0.000943	0.000929	0.001124
2 × 2 GI	1.13E−15	0.000327	0.000737	0.001603	0.000670	0.001759

Table 4
H^1 seminorm of error in the quadratic patch test for various methods and discretizations.

Method	β					
	0.0	0.2	0.4	0.6	0.8	1.0
1 × 1/2 × 2 GI	0.082208	0.089008	0.100639	0.170593	0.163169	0.199474
1 × 1/2 × 2 VC-GI	1.21E−14	0.008290	0.013081	0.018920	0.015366	0.019341
2 × 2 GI	1.03E−14	0.007693	0.013230	0.021340	0.014649	0.021676

seen that in the uniform case, 2 × 2 GI and 1 × 1/2 × 2 VC-GI are able to pass the patch test. However, in the non-uniform cases, no method is able to. This is because NURBS basis functions lack quadratic completeness in the spatial domain when weights are non-uniform or when the mapping is not affine, and thus they cannot exactly represent the solution. Nevertheless, the proposed 1 × 1/2 × 2 VC-GI method gives very similar levels of error as 2 × 2 GI for all discretizations. Additionally, given a discretization, it can be seen that GI with the variationally consistent approach can essentially eliminate the solution error induced by low order quadrature.

4.2. Poisson equation: convergence study

Consider the Poisson equation on $\Omega : (0, 1) \times (0, 1)$ with the solution $u = e^{xy}$:

$$\begin{aligned} &\nabla^2 u = (x^2 + y^2)e^{xy} \quad \text{in } \Omega \\ &u = e^{xy} \quad \text{on } \partial\Omega. \end{aligned} \tag{35}$$

First, quadratic NURBS are employed with a uniform discretization. Integration sufficient for convergence was found to be 2 × 2 GI in each cell, which was considered along with the proposed 1×1/2 ×2 VC-GI, and 1 × 1/2 × 2 GI for comparison. As seen in Fig. 5, 2 × 2 GI converges optimally (with a rate of 3 in the L^2 norm and 2 in the H^1 seminorm), 1 × 1/2 × 2 GI does not, and 1 × 1/2 × 2 VC-GI converges optimally in the H^1 seminorm and nearly

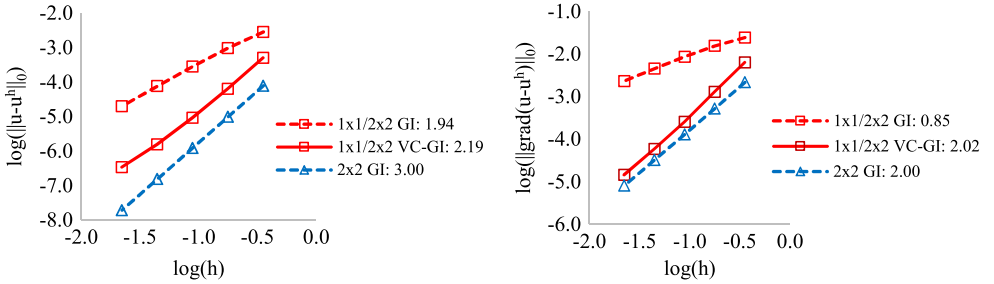

Fig. 5. Convergence of quadratic NURBS in uniform discretization of the Poisson problem.

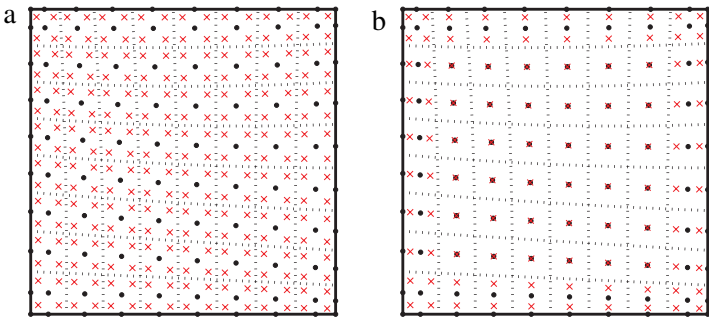

Fig. 6. Second refinement for non-uniform discretization of the Poisson problem for quadratic NURBS with (a) 2×2 GI and (b) $1 \times 1/2 \times 2$ GI. Black circles denote control points, red crosses integration points, and dashed lines integration cells.

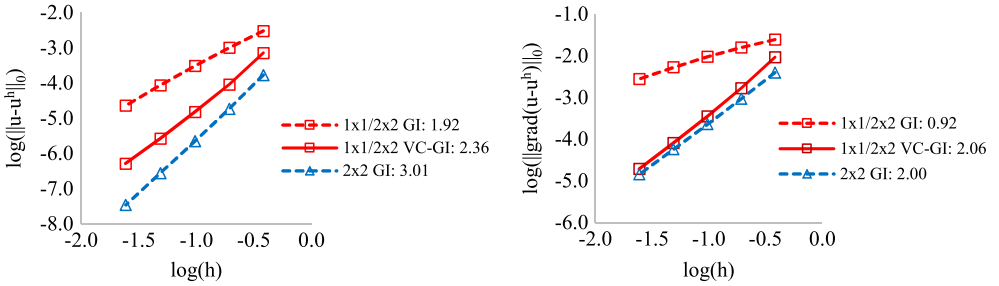

Fig. 7. Convergence of quadratic NURBS in non-uniform discretization of the Poisson problem.

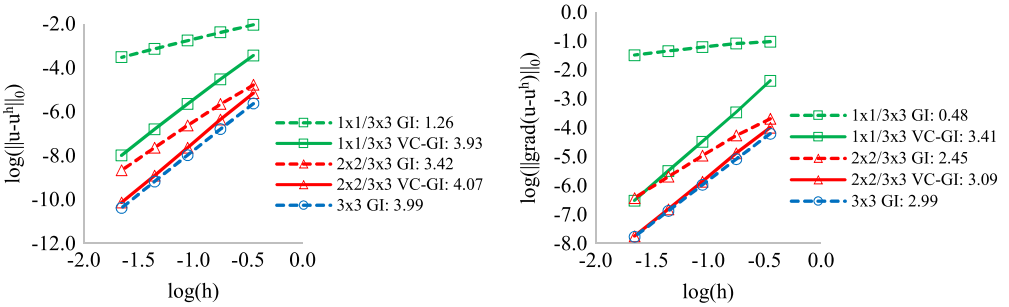

Fig. 8. Convergence of cubic NURBS in uniform discretization of the Poisson problem.

optimally in the L^2 norm. Here only one Gauss point per degree of freedom is used in the variationally consistent scheme, resulting in $1/4$ the number of quadrature points of 2×2 GI in the limit of discretization, with similar rates of convergence.

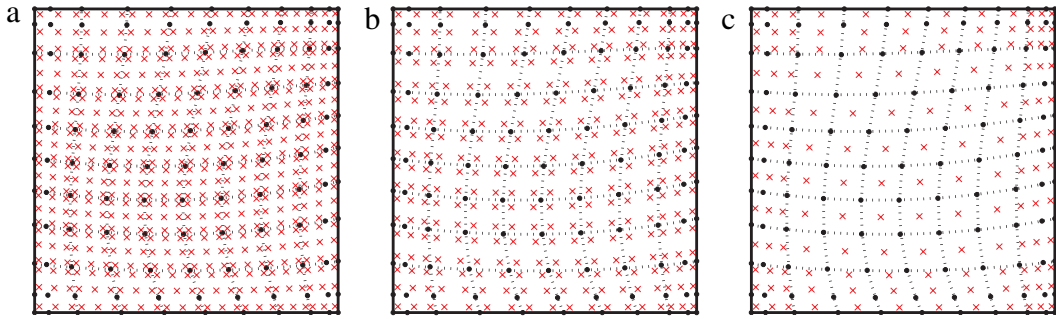

Fig. 9. Second refinement for non-uniform discretization of the Poisson problem for cubic NURBS with (a) 3×3 GI, (b) $2 \times 2/3 \times 3$ GI, and (c) $1 \times 1/3 \times 3$ GI. Black circles denote control points, red crosses integration points, and dashed lines integration cells.

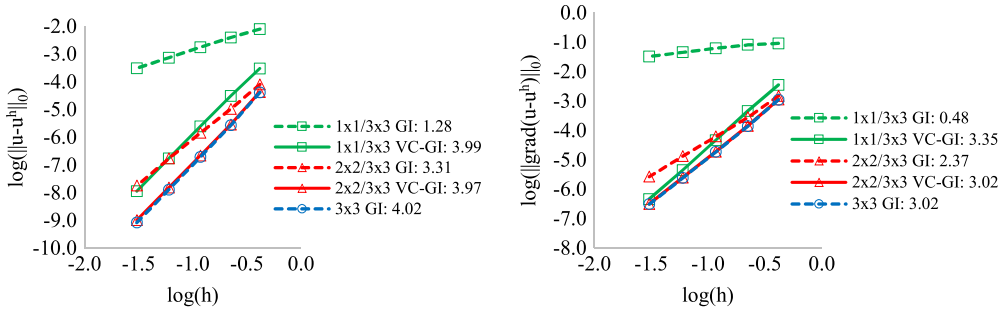

Fig. 10. Convergence of cubic NURBS in non-uniform discretization of the Poisson problem. Rates indicated in legend.

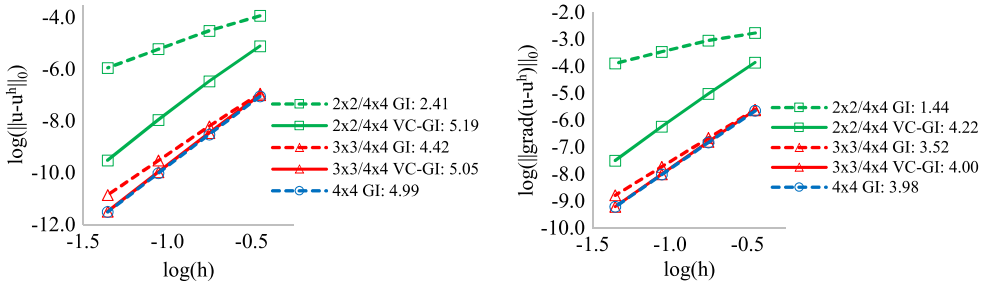

Fig. 11. Convergence of quartic NURBS in uniform discretization of the Poisson problem. Rates indicated in legend.

The discretization is perturbed with a factor $\beta = 0.3$ in the coarse discretization and refined uniformly, with the second refinement shown in Fig. 6. As seen in Fig. 7, non-optimal convergence is observed for $1 \times 1/2 \times 2$ GI, optimal convergence for 2×2 GI and optimal and nearly optimal convergence for $1 \times 1/2 \times 2$ VC-GI in the H^1 seminorm and L^2 norm, respectively. Again, roughly $1/4$ the number of quadrature points of 2×2 GI was used for the variationally consistent scheme, and similar rates of convergence were achieved.

Next, cubic NURBS are considered with a uniform discretization, with 3×3 GI, $2 \times 2/3 \times 3$ GI, and $1 \times 1/3 \times 3$ GI, along with VCI counterparts for the reduced quadrature cases. The VCI methods introduced are shown to provide the optimal convergence of 3×3 GI as seen in Fig. 8 (with rates of 4 and 3 in the L^2 norm and H^1 seminorm, respectively), while reduced quadrature without VCI does not. Here, the number of quadrature points for optimal convergence in $2 \times 2/3 \times 3$ VC-GI is less than one half ($4/9$) of that of 3×3 GI in the limit of discretization, and similar levels of error are achieved. The $1 \times 1/3 \times 3$ VC-GI method also provides optimal convergence rates with far fewer quadrature points than the p-points-per-cell rule ($1/9$ in the limit of discretization).

A non-uniform discretization with a factor $\beta = 0.3$ with cubic basis is then introduced with the schemes depicted in Fig. 9. As seen in Fig. 10, similar convergence rates are achieved again for the VCI methods and 3×3 GI, with the error levels even closer than the uniform case, while reduced quadrature without VCI again gives sub-optimal

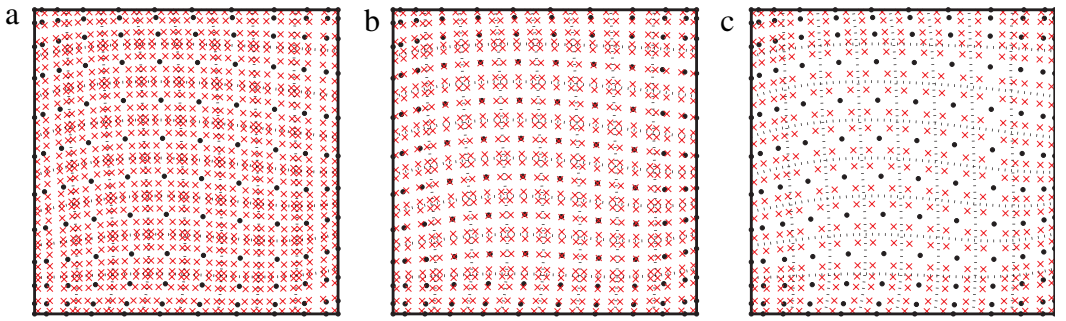

Fig. 12. Second refinement for non-uniform discretization of the Poisson problem for quartic NURBS with (a) 4×4 GI, (b) $3 \times 3/4 \times 4$ GI, and (c) $2 \times 2/4 \times 4$ GI. Black circles denote control points, red crosses integration points, and dashed lines integration cells.

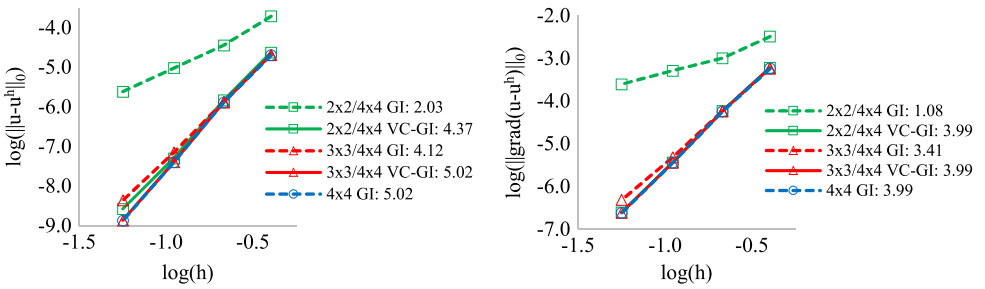

Fig. 13. Convergence of quartic NURBS in non-uniform discretization of the Poisson problem. Rates indicated in legend.

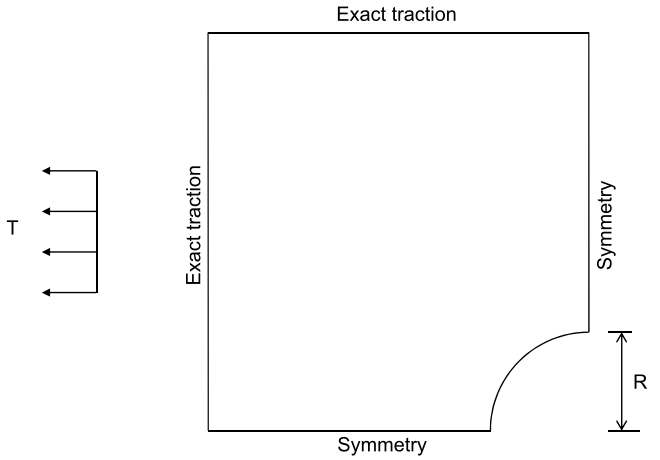

Fig. 14. Problem statement of infinite plate with circular hole.

rates with much larger error. Here it can also be seen that the same level of error as 3×3 GI can be achieved using $2 \times 2/3 \times 3$ VC-GI in both the H^1 seminorm and L^2 norm, and similar levels of error as 3×3 GI are achieved in the H^1 seminorm using $1 \times 1/3 \times 3$ VC-GI.

Quartic NURBS are also considered with a uniform discretization, with 4×4 GI, $3 \times 3/4 \times 4$ GI, $2 \times 2/4 \times 4$ GI, and their variationally consistent counterparts for reduced integration. As seen in Fig. 11, the proposed VCI methods give the optimal convergence of 4×4 GI (with rates of 5 and 4 in the L^2 norm and H^1 seminorm, respectively), with $3 \times 3/4 \times 4$ VC-GI giving the same level of error as well. As with the lower-order basis, the non-VC counterparts employed for reference fail to give optimal convergence.

A non-uniform discretization with a factor $\beta = 0.3$ shown in Fig. 12 is then introduced. As seen in Fig. 13, $3 \times 3/4 \times 4$ VC-GI gives optimal convergence with similar levels of error, and in the limit of refinement roughly half

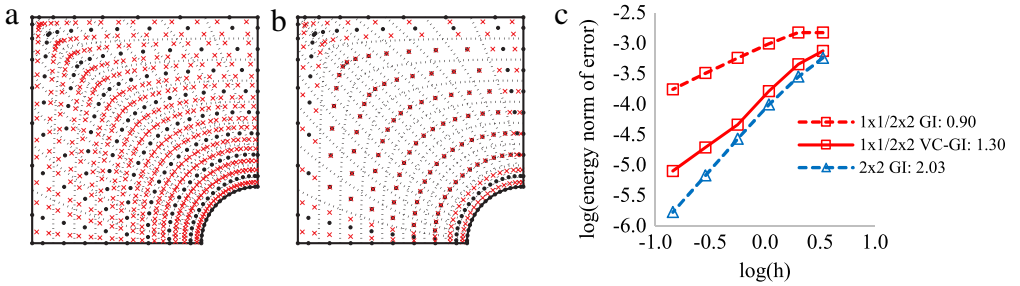

Fig. 15. Plate problem with quadratic NURBS: (a) Scheme for full 2×2 quadrature, (b) Scheme for reduced $1 \times 1/2 \times 2$ quadrature, and (c) Convergence in energy norm. Rates indicated in legend.

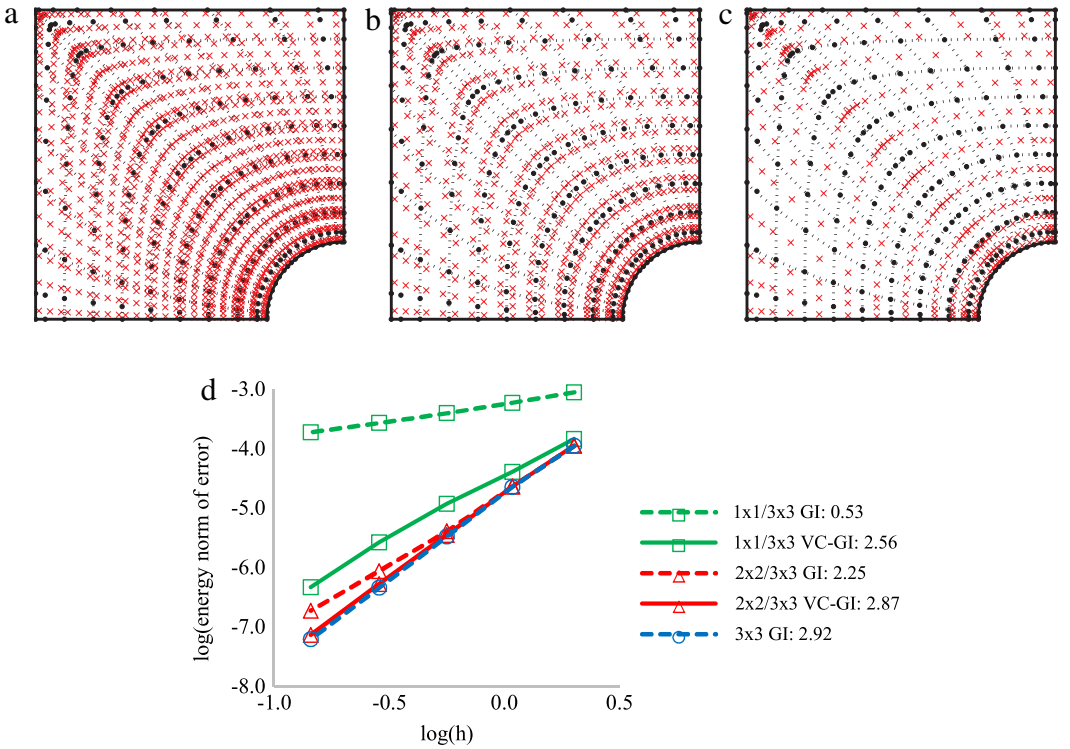

Fig. 16. Plate problem with cubic NURBS: (a) Scheme for full 3×3 quadrature, (b) Scheme for reduced $2 \times 2/3 \times 3$ quadrature, (c) Scheme for maximum reduced $1 \times 1/3 \times 3$ quadrature, and (d) Convergence in energy norm. Rates indicated in legend.

(9/16) the number of quadrature points are used than would otherwise be required. For $2 \times 2/4 \times 4$ VC-GI, similar levels of error are achieved, with optimal and near optimal rates of convergence for the H^1 seminorm and L^2 norm, respectively. As with the lower order basis in non-uniform discretizations, optimal convergence and very similar levels of error are achieved in the derivatives using fully reduced quadrature with VCI.

4.3. Elastostatics: infinite plate with circular hole

An infinite plate with a hole subject to uniaxial tension shown in Fig. 14 is considered, with loading, geometric, and material values $R = 1.0$ in, $T = 10.0$ psi, $E = 30.0 \times 10^6$ psi, and $\nu = 0.3$. The problem is modeled with symmetry of the upper left quadrant, with exact traction prescribed along a square portion of the domain of length 4.0 in.

Quadratic NURBS are employed with the previously considered integrations, shown with the second refinement in Fig. 15(a) and (b). As seen in Fig. 15(c), the convergence rate in the energy norm is quite low for $1 \times 1/2 \times 2$ GI, optimal for 2×2 GI, and much better for $1 \times 1/2 \times 2$ VC-GI with similar levels of error achieved as 2×2 GI.

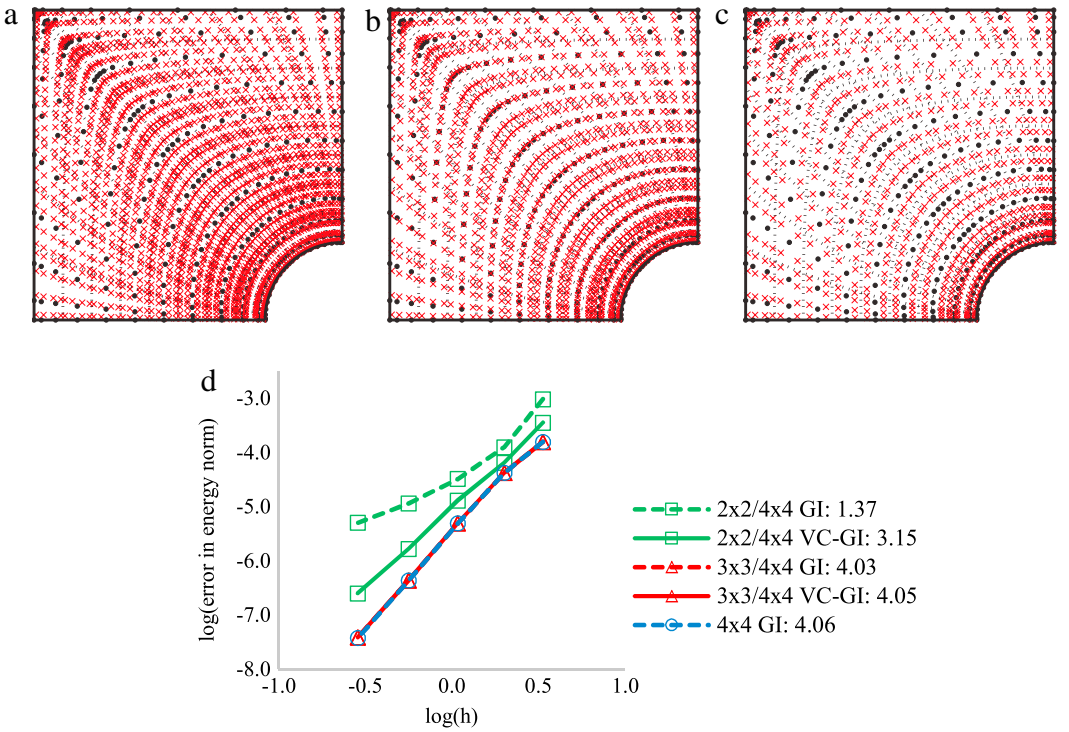

Fig. 17. Plate problem with quartic NURBS: (a) Scheme for full 4×4 quadrature, (b) Scheme for reduced $3 \times 3/4 \times 4$ quadrature, (c) Scheme for further reduced $2 \times 2/4 \times 4$ quadrature, and (d) Convergence in energy norm. Rates indicated in legend, calculated using $h = 1/\sqrt{NP}$ due to the spacing in the discretization.

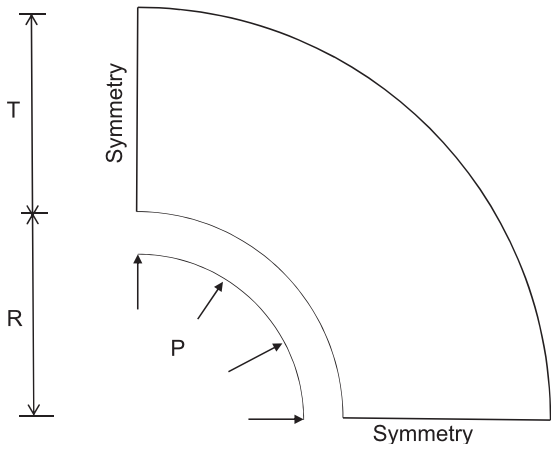

Fig. 18. Problem statement of infinitely long hollow thick pipe under internal pressure.

Cubic NURBS are then introduced with the integration schemes shown with the second refinement in Fig. 16(a)–(c). Note that for this discretization there is a repeated knot in the ξ direction, and cells adjacent to the associated line are integrated with $p \times p$ points per cell. Fig. 16(d) shows VCI can provide near optimal convergence, with similar levels of error achieved as 3×3 GI.

Finally, quartic NURBS are considered with the previously introduced integration schemes, shown with the second refinement in Fig. 17(a)–(c). Note that again a repeated knot in the ξ direction exists. The results in Fig. 17(d) show that the solution error for $3 \times 3/4 \times 4$ GI is negligible, and, as a result, in this case VCI does not improve the

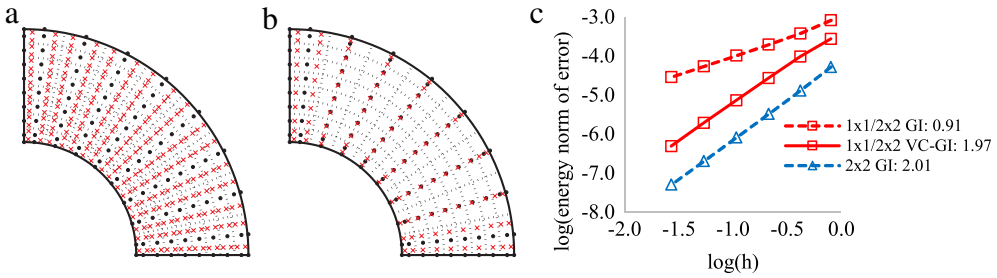

Fig. 19. Pipe problem with quadratic NURBS: (a) VCI scheme for full 2×2 quadrature, (b) scheme for reduced $1 \times 1/2 \times 2$ quadrature, and (c) Convergence in the energy norm.

convergence rates. The $2 \times 2/4 \times 4$ VC-GI method on the other hand can provide similar rates of convergence and similar levels of error, while, as before, its variationally inconsistent counterpart does not.

4.4. Elastostatics: infinitely long hollow thick pipe under internal pressure

The infinitely long hollow pipe problem in Fig. 18 is considered with loading, geometric, and material values $R = 1.0$ in, $T = 1.0$ in, $P = 20.0$ psi, $E = 30.0 \times 10^6$ psi, and $\nu = 0.3$. The problem is modeled with symmetry of upper right quadrant. First, quadratic NURBS are considered with the integration schemes shown with the second refinement in Fig. 19(a)–(c). Convergence in the energy norm is shown in Fig. 19(d), where it is seen that optimal convergence of 2×2 GI is achieved for the $1 \times 1/2 \times 2$ VC-GI case.

Cubic NURBS are considered next with the quadrature schemes shown with the first refinement in Fig. 20(a)–(c). Convergence in the energy norm is shown in Fig. 20(d), where it is seen that 3×3 GI and the proposed VCI schemes exhibit optimal convergence and $2 \times 2/3 \times 3$ GI and $1 \times 1/3 \times 3$ GI employed for reference give much lower, suboptimal rates. Here, in coarser discretizations it is seen that the correction of $2 \times 2/3 \times 3$ GI gives slightly larger error, which may be due to the employment of an incomplete approximation. In coarse discretizations the lack of completeness is more significant and is thus more likely to adversely affect the use of VCI which is based on complete approximation spaces.

Quartic NURBS are then considered with the integration schemes shown with the second refinement in Fig. 21(a)–(c). The results in Fig. 21(d) show that optimal convergence is attained with 4×4 GI and the VCI methods, while the convergence rate for $3 \times 3/4 \times 4$ GI is not completely full and very low for $2 \times 2/4 \times 4$ GI. It is again seen in this case that the error can be slightly worse for VCI in coarse discretizations, again likely due to the reasons discussed above.

5. Conclusions

The straightforward Gaussian quadrature using cells defined by knots spans in IGA provides sufficient accuracy and optimal convergence, but is inefficient for the approximation functions at hand. Constructions of test function gradients based on the variational consistency conditions have been introduced, which allows a significant reduction in the number of quadrature points used without sacrificing accuracy, stability, and optimal convergence of IGA. The rules introduced use low-order Gaussian quadrature ($p-1$ or $p-2$ points) on the interior, and p integration points in cells adjacent to repeated knots, for NURBS constructed from B-splines of degree p. The lack of global completeness in the physical domain of the NURBS bases does not in general adversely affect the results.

The proposed method gives similar levels of error as higher order integration (p points per cell), with optimal or near optimal convergence rates being attained for all cases tested. One interesting result is that quadratic NURBS with VCI gives optimal or near optimal convergence in the H^1 seminorm and gives roughly the same level of error as 2×2 integration, using only one quadrature point per basis function. As such, the method is comparable to a collocation technique in terms of computational cost. For higher order bases, optimal or near optimal convergence is attained for $p-1$ and $p-2$ points per cell in both the solution and its derivatives, with the similar levels of error as higher-order quadrature using p points per cell. An attractive feature of the proposed VCI method is that it is straightforward to implement, and is applicable to arbitrary non-uniform NURBS discretizations, and thus warrants investigation for other classes of IGA approximations and beyond.

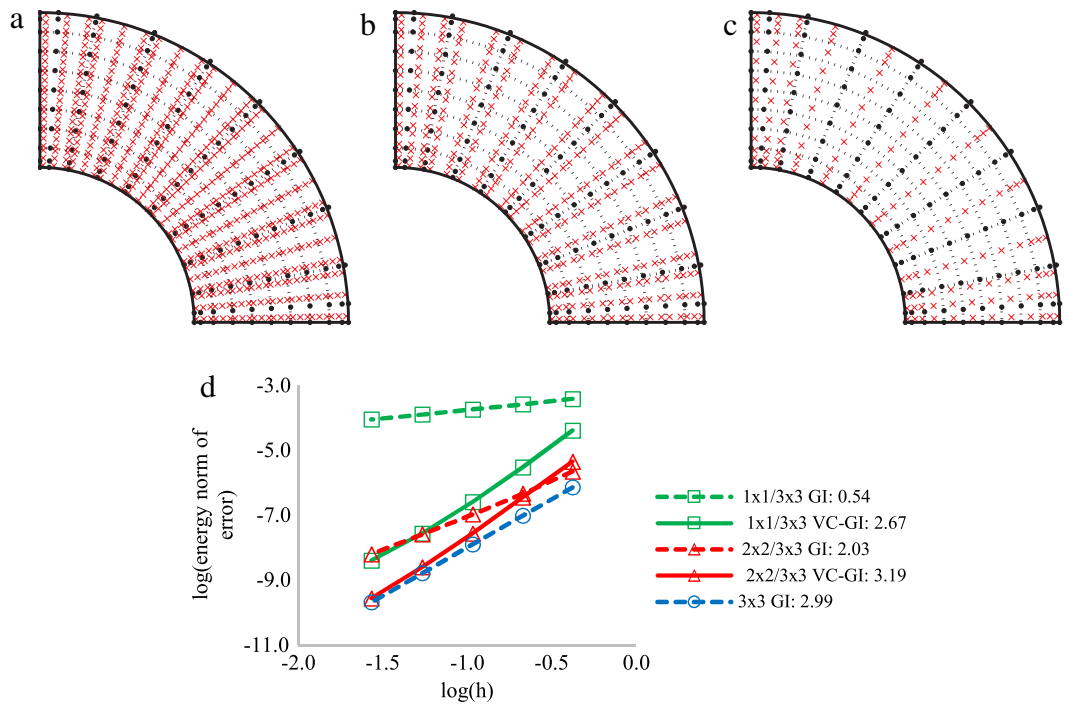

Fig. 20. Pipe problem with cubic NURBS: (a) Scheme for full 3×3 quadrature, (b) Scheme for reduced $2 \times 2/3 \times 3$ quadrature, (c) Scheme for maximum reduced $1 \times 1/3 \times 3$ quadrature, and (d) Convergence in the energy norm.

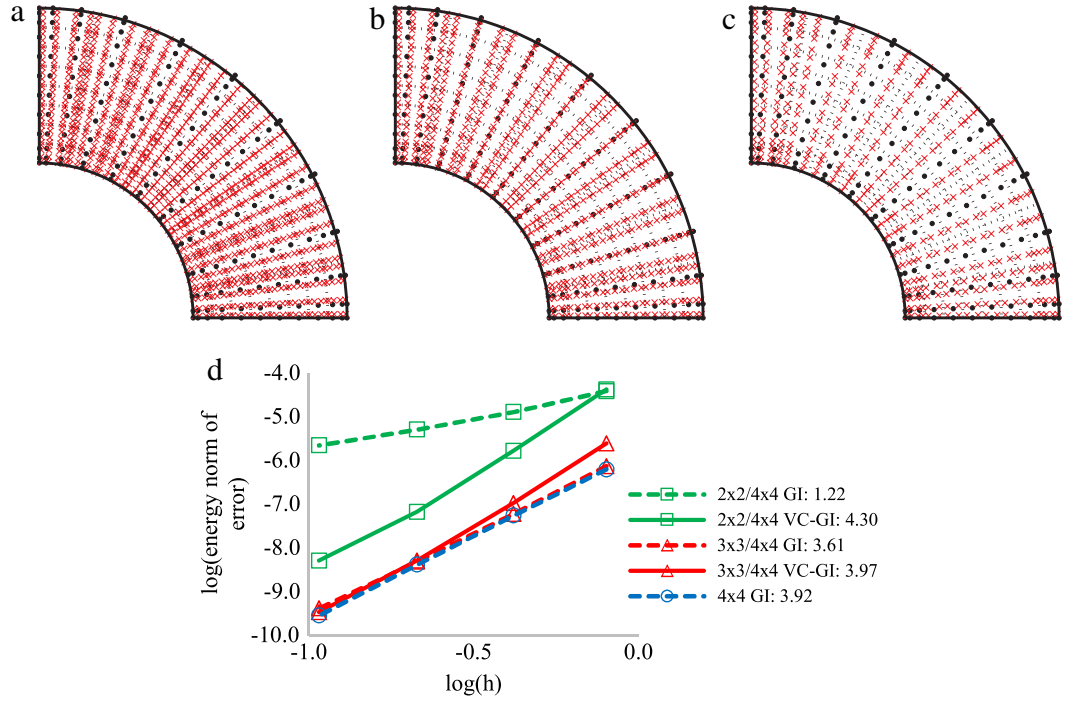

Fig. 21. Pipe problem with quartic NURBS: (a) Scheme for full 4×4 quadrature, (b) Scheme for reduced $3 \times 3/4 \times 4$ quadrature, (c) Scheme for further reduced $2 \times 2/4 \times 4$ quadrature, and (d) Convergence in the energy norm.

Acknowledgments

The support of this work by US Army Engineer Research and Development Center under contract W912HZ-07-C-0019 to the first and second authors and by AFOSR under contract FA9550-12-1-0005 to the third author is greatly acknowledged.

References

[1] T.J.R. Hughes, J.A. Cottrell, Y. Bazilevs, Isogeometric analysis: CAD, finite elements, NURBS, exact geometry, and mesh refinement, Comput. Methods Appl. Mech. Engrg. 194 (2005) 4135–4195.
[2] J.A. Cottrell, T.J.R. Hughes, Y. Bazilevs, Isogeometric Analysis: Toward Integration of CAD and FEA, John Wiley & Sons, Ltd., New York, NY, 2009.
[3] L. Beirão da Veiga, A. Buffa, J. Rivas, G. Sangalli, Some estimates for $h-p-k$ refinement in isogeometric analysis, Numer. Math. 118 (2) (2011) 271–305.
[4] T.J.R. Hughes, A. Reali, G. Sangalli, Duality and unified analysis of discrete approximations in structural dynamics and wave propagation: comparison of p-method finite elements with k-method NURBS, Comput. Methods Appl. Mech. Engrg. 197 (2008) 4104–4124.
[5] T.J.R. Hughes, A. Reali, G. Sangalli, Efficient quadrature for NURBS- based isogeometric analysis, Comput. Methods Appl. Mech. Engrg. 199 (2010) 301–313.
[6] F. Auricchio, F. Calabrò, T.J.R. Hughes, A. Reali, G. Sangalli, A simple algorithm for obtaining nearly optimal quadrature rules for NURBS-based isogeometric analysis, Comput. Methods Appl. Mech. Engrg. 249 (2012) 15–27.
[7] Y. Bazilevs, V.M. Calo, J.A. Cottrell, J. Evans, T.J.R. Hughes, S. Lipton, M.A. Scott, T.W. Sederberg, Isogeometric analysis using T-Splines, Comput. Methods Appl. Mech. Engrg. 199 (2010) 229–263.
[8] N. Nguyen-Thanh, J. Kiendl, H. Nguyen-Xuan, R. Wüchner, K.U. Bletzinger, Y. Bazilevs, T. Rabczuk, Rotation free isogeometric shell analysis using PHT-splines, Comput. Methods Appl. Mech. Engrg. 200 (47–48) (2011) 3410–3424.
[9] K.A. Johannessen, T. Kvamsdal, T. Dokken, Isogeometric analysis using LR B-splines, Comput. Methods Appl. Mech. Engrg. 269 (2014) 471–514.
[10] J.S. Chen, C.T. Wu, S. Yoon, Y. You, A stabilized conforming nodal integration for Galerkin mesh-free methods, Internat. J. Numer. Methods Engrg. 50 (2001) 435–466.
[11] Q. Duan, X. Li, H. Zhang, T. Belytschko, Second-order accurate derivatives and integration schemes for meshfree methods, Internat. J. Numer. Methods Engrg. 92 (2012) 399–424.
[12] J.S. Chen, M. Hillman, M. Rüter, An arbitrary order variationally consistent integration method for Galerkin meshfree methods, Internat. J. Numer. Methods Engrg. 95 (2013) 387–418.
[13] J.S. Chen, S. Yoon, C.T. Wu, Nonlinear version of stabilized conforming nodal integration for Galerkin meshfree methods, Internat. J. Numer. Methods Engrg. 53 (2002) 2587–2615.
[14] D. Wang, J.S. Chen, Locking-free stabilized conforming nodal integration for meshfree Mindlin–Reissner plate formulation, Comput. Methods Appl. Mech. Engrg. 193 (2004) 1065–1083.
[15] D. Wang, J.S. Chen, A Hermite reproducing kernel approximation for thin-plate analysis with sub-domain stabilized conforming integration, Internat. J. Numer. Methods Engrg. 74 (2008) 368–390.
[16] J.S. Chen, D. Wang, A constrained reproducing kernel particle formulation for shear deformable shell in Cartesian coordinates, Internat. J. Numer. Methods Engrg. 68 (2006) 151–172.
[17] J.W. Yoo, B. Moran, J.S. Chen, Stabilized conforming nodal integration in the natural-element method, Internat. J. Numer. Methods Engrg. 60 (2004) 861–890.
[18] H.Y. Hu, J.S. Chen, W. Hu, Weighted radial basis collocation method for boundary value problems, Internat. J. Numer. Methods Engrg. 69 (2007) 2736–2757.
[19] J.S. Chen, W. Hu, H.Y. Hu, Reproducing kernel enhanced local radial basis collocation method, Internat. J. Numer. Methods Engrg. 75 (2008) 600–627.
[20] D. Schillinger, J.A. Evans, A. Reali, M.A. Scott, T.J.R. Hughes, Isogeometric collocation: cost comparison with Galerkin methods and extension to adaptive hierarchical NURBS discretizations, Comput. Methods Appl. Mech. Engrg. 267 (2013) 170–232.
[21] D. Wang, H. Zhang, A consistently coupled isogeometric–meshfree method, Comput. Methods Appl. Mech. Engrg. 268 (2014) 843–870.
[22] Y. Bazilevs, L. Beirao da Veiga, J.A. Cottrell, T.J.R. Hughes, G. Sangalli, Isogeometric analysis: Approximation, stability and error estimates for h-refined meshes, Math. Models Methods Appl. Sci. 16 (2006) 1031–1090.
[23] Nitsche J, Über ein Variationsprinzip zur Lösung von Dirichlet-Problemen bei Verwendung von Teilräumen, die keinen Randbedingungen unterworfen sind, Abh. Math. Semin. Univ. Hambg. 36 (1971) 9–15.